TISSUE ENGINEERING: Part A
Volume 22, Numbers 19 and 20, 2016

DOI: 10.1089/ten.tea.2016.0134

termis
Tissue Engineering
& Regenerative Medicine
International Society

ORIGINAL ARTICLE

Codelivery of Infusion Decellularized Skeletal Muscle with Minced Muscle Autografts Improved Recovery from Volumetric Muscle Loss Injury in a Rat Model

Benjamin Kasukonis, MS,[1] John Kim, BS,[1] Lemuel Brown, MS,[2] Jake Jones, BS,[1] Shahryar Ahmadi, MD,[3] Tyrone Washington, PhD,[2] and Jeffrey Wolchok, PhD[1]

Skeletal muscle is capable of robust self-repair following mild trauma, yet in cases of traumatic volumetric muscle loss (VML), where more than 20% of a muscle's mass is lost, this capacity is overwhelmed. Current autogenic whole muscle transfer techniques are imperfect, which has motivated the exploration of implantable scaffolding strategies. In this study, the use of an allogeneic decellularized skeletal muscle (DSM) scaffold with and without the addition of minced muscle (MM) autograft tissue was explored as a repair strategy using a lower-limb VML injury model ($n = 8$/sample group). We found that the repair of VML injuries using DSM + MM scaffolds significantly increased recovery of peak contractile force ($81 \pm 3\%$ of normal contralateral muscle) compared to unrepaired VML controls ($62 \pm 4\%$). Similar significant improvements were measured for restoration of muscle mass ($88 \pm 3\%$) in response to DSM + MM repair compared to unrepaired VML controls ($79 \pm 3\%$). Histological findings revealed a marked decrease in collagen dense repair tissue formation both at and away from the implant site for DSM + MM repaired muscles. The addition of MM to DSM significantly increased *MyoD* expression, compared to isolated DSM treatment (21-fold increase) and unrepaired VML (37-fold) controls. These findings support the further exploration of both DSM and MM as promising strategies for the repair of VML injury.

Introduction

Our group is exploring the development of strategies designed to treat volumetric muscle loss (VML) injuries. The substantial loss (>20%) of skeletal muscle tissue, either through trauma or surgical resection, appears to overwhelm the normal wound healing mechanisms that function effectively following minor muscle injuries.[1] It is generally recognized that to properly restore muscle function following VML injury, surgical intervention is required. Unfortunately, there are limited surgical options available to treat these clinically challenging VML injuries. The currently accepted surgical approach for the replacement of lost skeletal muscle is autologous muscle flap transfer.[2–4] Although frequently successful, muscle flap transfer is a highly invasive procedure that introduces significant donor site morbidity and is, therefore, only rarely indicated. The search for a less invasive VML repair strategy warrants research investment. Toward this end, several groups, including ours, are exploring the development of engineered extracellular matrix (ECM) scaffolds targeting VML repair.[5–9]

ECM scaffolds prepared from a variety of tissue sources have been utilized to repair a wide range of damaged tissues in animal models[10–13] and recently in humans.[14,15] Within this class of tissue-derived ECM scaffolds, the application of decellularized skeletal muscle (DSM) as a repair strategy for VML injury has shown some promise.[11,13] The multimolecular composition and highly aligned network architecture of DSM scaffolds are ideally suited for the restoration of physical and chemical cues that are lost following VML injury. To improve the preparation of DSM scaffolds, our group has recently reported on a novel infusion method, which can accelerate the decellularization process, without compromising the physical, chemical, and biocompatibility properties.[16] Our goal is to explore the utility of these infusion prepared DSM scaffolds for the repair of VML injuries. Yet, the implantation of DSM scaffolds alone, particularly when explored in the lower extremity, appears to offer an incomplete intervention for the repair of VML injuries,[17] suggesting that other elements may be needed.

Evidence suggests that restoration of a robust pro-myogenic environment may require a multifactorial approach, which

[1]Department of Biomedical Engineering, College of Engineering, University of Arkansas, Fayetteville, Arkansas.
[2]Department of Health, Human Performance, and Recreation, College of Education and Health Professions, University of Arkansas, Fayetteville, Arkansas.
[3]Department of Orthopedics, University of Arkansas for Medical Sciences, Little Rock, Arkansas.

includes combining ECM scaffolds with the appropriate progenitor cells. In animal studies, the codelivery of muscle progenitor cells in combination with ECM scaffolds has been shown to improve functional recovery following VML injury compared to ECM scaffold delivery alone.[10,11] The premise is that progenitor cells reestablish a needed pool of myogenic cells, which utilize the ECM implant as a substrate upon which to initiate regeneration of contractile myofibers. Cellular codelivery has yielded promising VML regenerative results, but does introduce increased clinical complexity, as it would require surgical collection and expansion of the patient's progenitor cells before implantation. Our group is interested in exploring alternatives to *in vitro* progenitor cell expansion and cultivation, with the aim of creating a single-stage VML repair strategy. An attractive source of muscle progenitor cells is the collection and implantation of minced muscle (MM) autografts. MM contains several components, most notably satellite cells, necessary for the regeneration of skeletal muscle and has been shown to successfully regenerate damaged muscle tissue when examined in animal models of VML injury.[18,19] Of particular interest to our group, MM autografts can be harvested from normal muscle tissue and seeded back into the injury site during a single-stage surgical procedure.

An anticipated roadblock to the clinical translation of MM autografts is the large volume of healthy muscle tissue that would be needed for grafting into a VML defect. At present, the implantation of MM in quantities prepared using <50% of the VML defect mass has not been effective at restoring muscle function.[19] While potentially less invasive than a full muscle flap transfer, the harvest of muscle tissue in volumes required to fill half the VML defect would still introduce significant donor site morbidity. Therefore, a repair strategy that reduces the amount of MM needed to stimulate functional muscle recovery would improve the clinical utility of MM autografts. Toward this end, our team is interested in exploring the codelivery of MM autografts with infusion prepared DSM scaffolds as a VML repair strategy. We suspect that the use of DSM material as a carrier material could reduce the amount of MM autografts needed to stimulate recovery following VML injury. Specifically, the study was designed to test the hypothesis that delivery of a DSM scaffold carrier combined with a MM autograft prepared using 25% of the defect mass (1/2 the current threshold for recovery) will significantly improve functional muscle recovery (increased contractile force) and myogenesis (increased MyoD expression) following hind limb VML injury in a small animal model.

Methods

DSM scaffold preparation

To prepare DSM samples for implantation, whole tibialis anterior (TA) muscle was infusion decellularized using the previously reported[16] infusion system (Fig. 1). TA muscles were harvested from rats that had been euthanized at the completion of an unrelated study. Briefly, the wide mid-belly region of the TA muscle was positioned onto the infusion needle (27 gauge) and enclosed within a single decellularization chamber. Four TA muscles were prepared in parallel during each run. The TA samples were infused overnight ($\sim$12 h) with 1% sodium dodecyl sulfate at a flow rate of 5 mL/h. Following infusion treatment, samples were incubated overnight in a DNAse solution (1 kU/mL DNAse in a 10 mM Tris-HCL buffer; 2.5 mM $MgCL_2$ + 0.5 mM $CaCl_2$) and then incubated (8 h) in a 1× penicillin/streptomycin solution to reduce the risk of infection. Samples were rinsed thoroughly (a total of six 24 h wash steps) in phosphate-buffered saline (PBS) between each preparation step. Following completion of the entire decellularization protocol, the DNA concentration of representative DSM implants ($n = 4$) was measured with the aid of a commercial quantification kit (Qubit; Fisher Scientific). DSM implants were lyophilized and stored at −20°C until utilized for implantation.

Animal implantation

Fischer 344 rats (Harlan), weighing $\sim$300–325 g, were used as the animal model for all implantation studies. Surgical procedures and DSM implant preparation methods were performed in accordance with protocols approved by the University of Arkansas IACUC (protocol #14044) and guided by published methods.[20,21] Anesthesia was induced using isoflurane (1–3%) in oxygen. The implant site was surgically exposed through a 1–2 cm incision running parallel to the tibia. The TA was identified and a partial thickness VML defect (8 mm diameter × 3 mm deep) was created using a sterile biopsy punch (Fig. 2). The muscle tissue removed from the defect site was weighed and the weight was adjusted (increased only) if needed to ensure consistent defect mass across all animals (average defect weight = 93.4 mg). Muscle defect mass values (20% of TA mass) were based on pilot study TA muscle mass measurements (average TA mass = 470 ± 17 mg). Muscle defect plugs were retained for use as MM autografts. Animals were randomly assigned to one of three treatment groups ($n = 8$ animals/treatment groups)

Group 1: Unrepaired VML defect

Group 2: VML defect repaired with an isolated DSM scaffold

Group 3: VML defect repaired with a DSM scaffold supplemented with MM autograft tissue (25% of the VML defect mass)

A single infusion-prepared DSM scaffold was cut to size (average DSM mass = 4.9 ± 0.7 mg) using surgical scissors and implanted into freshly prepared VML defects (Group 2). For animals in the DSM + MM experimental group (Group 3), 25% of the defect muscle plug was hand minced into a loose paste using a scalpel and scissors until MM fragments larger than $\sim$1 mm^3 could not be visually detected. The white DSM scaffolds were manually rolled in the pink MM autograft paste until all surfaces were visibly coated. DSM + MM constructs were implanted into the VML defect. Care was taken to ensure that DSM implant network alignment was matched to TA alignment. Unrepaired VML defects (group 1) served as negative controls ($n = 8$/experimental group). The contralateral limb was left untreated to serve as an internal comparative control. To remain consistent with previous MM repair techniques, the DSM scaffolds were sized to fill, but were not sutured to the surrounding muscle tissue. The deeper fascia and surface skin layers were separately closed using an interrupted stitch with a 5-0 absorbable suture (Vicryl; Ethicon). A single surgeon (B.K.) performed all implantation procedures, including the preparation of MM autografts. Postoperative analgesia consisted of 0.1 mg/kg buprenorphine administered

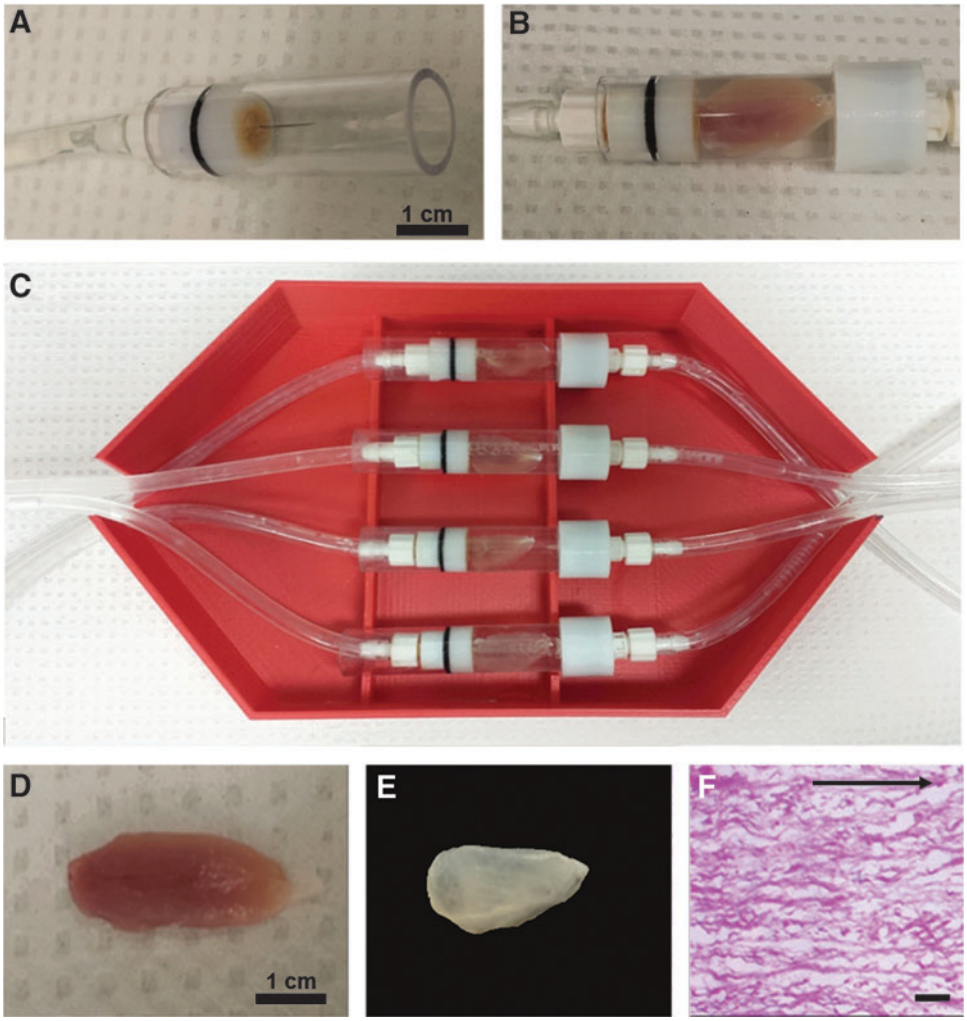

FIG. 1. DSM scaffolds were infusion decellularized using a custom-built infusion bioreactor. During decellularization, SDS solution was delivered using a hypodermic needle **(A)**, which was positioned into the wide mid-belly region of the TA muscle **(B)**. SDS solution was infused using a syringe pump (5 mL/h for 12 h) through each muscle and outflowed to waste collection. The bioreactor was designed to accommodate four side-by-side decellularization units each capable of accommodating a single muscle tissue sample **(C)**. Representative whole TA muscle appearance before and following infusion decellularization treatment **(D, E)** illustrates the dramatic color change (*red* to *white*) following removal of intracellular myoglobin. Infusion prepared DSM scaffolds, when viewed in thin section (scale bar = 100 μm) with hematoxylin and eosin staining, retained the highly aligned architecture of native muscle ECM **(F)**. (*arrow* = direction of contraction). DSM, decellularized skeletal muscle; SDS, sodium dodecyl sulfate; TA, tibialis anterior; ECM, extracellular matrix. Color images available online at www.liebertpub.com/tea

subcutaneously through injection twice daily for 2 days. Animals also had access to the anti-inflammatory medication (Carprofen) using a single dietary gel cup (MediGel CPF; ClearH_2O) added to each cage following surgery. Animal consumption of the gel was voluntary and any uneaten gel was removed from the cage at 1-week postsurgery. Following surgery, animals were housed in standard-sized rat cages with unrestricted movement. The animals were allowed to bear weight on the operative extremity as tolerated. All animals were housed for a 12-week recovery period.

Contractile force measurement

At the completion of the 12-week recovery period, the peak tetanic contractile force was measured *in situ* as described in Corona *et al.*[18] Animals were anesthetized and the lower limb was stabilized at 90° of knee flexion (tibia parallel to the benchtop) using a custom-made alignment jig (Supplementary Fig. S1; Supplementary Data are available online at www.liebertpub.com/tea). The ankle was flexed to 90° and the foot was secured (surgical tape) to the lever arm of a dual-mode muscle lever system (Aurora Scientific). To isolate the contribution of the TA during force measurement, distal tenotomies were performed on the extensor digitorum longus (EDL) and extensor hallucis longus. TA peak isometric tetanic force was measured by stimulating the peroneal nerve with the aid of a physiological stimulator (Grass; S88). Optimal voltage (2–5 V) was determined using a series of tetanic contractions (150 Hz, 0.1 ms pulse width, 400 ms train). Average peak tetanic force for each animal was calculated from an average of five contractions. All contractions were separated by 1 min of rest. Raw peak tetanic contractile force (N) was recorded from both the treated and contralateral control limb of each animal and normalized to animal weight (N/kg). The weight normalized force data (N/kg) are reported in the results section. At the conclusion of electrophysiological testing, all animals were euthanized through carbon dioxide inhalation in accordance with guidelines provided by the 2013 AVMA Panel on Euthanasia of Animals.

Tissue histology

Unrepaired and repaired TA muscles along with contralateral untreated TA muscles were harvested and trimmed to remove the periosteum and tendon. EDL muscles were also collected and weighed for comparison between treated and contralateral control limbs. Muscles were rinsed in sterile PBS, dabbed dry, and then weighed. Muscles were then immediately flash frozen in liquid nitrogen cooled isopentane.

Frozen TA tissue samples ($n=4$/experimental group) were sectioned (7 μm) transversely through the mid-portion of the defect site with the aid of a cryostat. Sections were mounted onto microscopic slides and immunostained for the presence of myosin heavy chain (αMHC, 1:40; Iowa Hybridoma Bank), a muscle-specific protein marker, collagen type I (αColI, 1:750; Sigma), collagen type III (αColIII, 1:000; Abcam), or laminin 1 (500:1; Sigma) followed by incubation in the appropriate fluorescently labeled secondary antibodies (Alexa Fluor, 500:1; Life Technologies). Additional tissue sections were stained using a commercial Masson's Trichrome Kit following manufacturer's guidelines (Sigma). All sections were mounted onto microscope slides and digitally imaged. Treated sections were evaluated for myofiber formation and organization, as well as the formation and extent of repair tissue formation, for comparison to untreated contralateral muscle tissue sections.

Measures of αColI accumulation, a potential indicator of diffuse muscle fibrosis, in tissue regions away from the VML defect area were estimated from collagen I immunoreactivity and guided by published methods.[22] Tissue immunoreactivity to collagen I was calculated from fluorescent microscopic images (200×) using image analysis software (ImageJ). A total of three nonconsecutive tissue sections collected from three representative animals ($n=3$/treatment group) were used for all calculations. From each section, three images were obtained from the posterior half of the TA muscle at regions located distant to (>3 mm) the anterior defect/repair site. A total of nine images were analyzed for each animal. All images were converted to 8-bit, gray scale, and uniformly thresholded across all samples to isolate αColI positive tissue regions. From these images, the percent αColI positive tissue area was calculated for all treatment and control sections.

MyoD and ECM gene expression

Real-time polymerase chain reaction (RT-PCR) was performed using the protocol described in Washington *et al.*[23] Tissue samples (~30 mg) collected from the defect/repair site ($n=4$/sample group) were homogenized with TRIzol (Ambion) and chloroform (Sigma Aldrich) and treated with DNase (Invitrogen). RNA was extracted using the RNeasy Kit (Invitrogen). RNA concentration and purity were determined by UV spectrophotometry. RNA with a 260-to-280-nm ratio ≥1.8 was used for subsequent analysis. cDNA was reverse transcribed from 1 μg of total RNA using the SuperScript VILO cDNA Synthesis Kit (Life Technologies). cDNA was amplified in a 25 μL reaction containing appropriate primer pairs and TaqMan Universal Master Mix (Applied Biosystems). Commercially available TaqMan primers (Invitrogen) for *MyoD*,

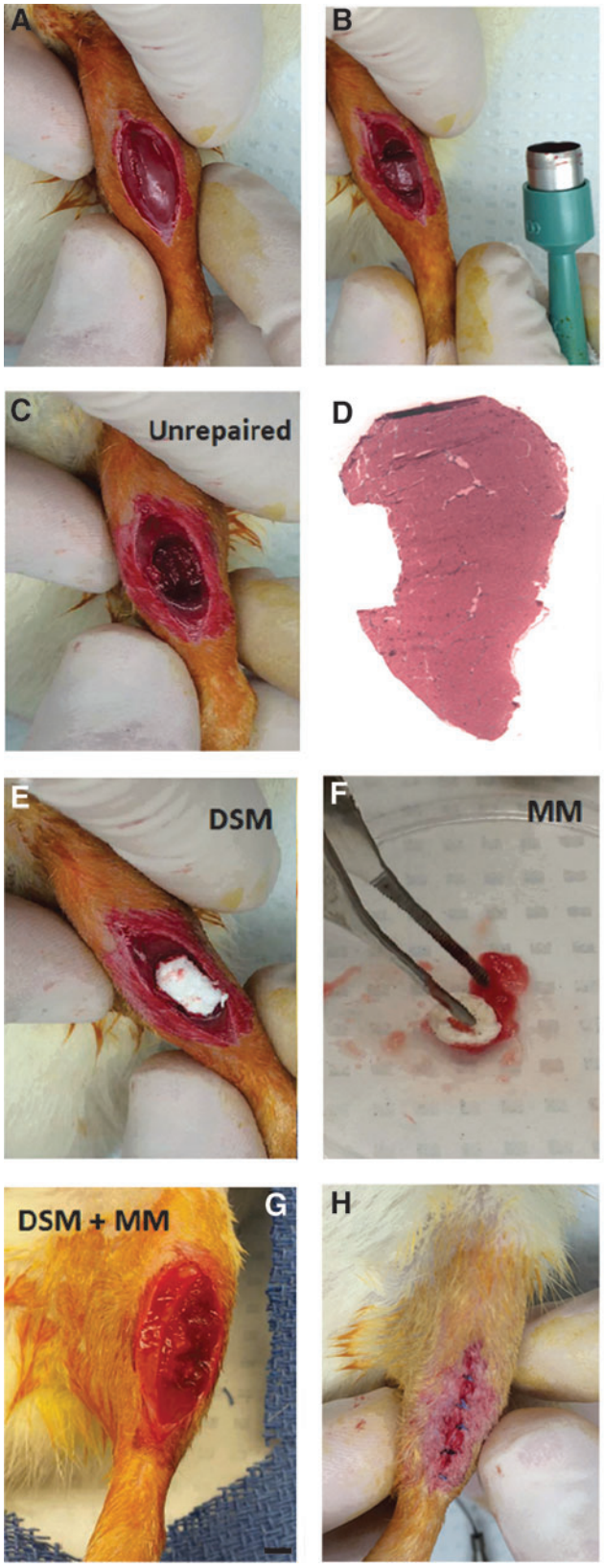

FIG. 2. To create the VML injury model, the mid-belly region of the TA muscle in a Fischer 344 rat was visualized through a 1–2 cm incision **(A)** and ~20% of the TA muscle (average defect weight = 94 ± 6 mg) was excised using an 8 mm biopsy punch inserted to a depth of 3 mm **(B–D)**. During isolated DSM repair, a single scaffold was cut to size and implanted into the TA defect **(E)**. To prepare each MM autograft, 25% of the previously removed defect plug was minced with a scalpel and scissors and then used to coat the surface of a single DSM scaffold **(F)**. The combined DSM scaffold and MM paste construct were implanted into the TA defect **(G)**. The deep fascia and skin **(H)** were closed separately using absorbable sutures. VML, volumetric muscle loss; MM, minced muscle. Color images available online at www.liebertpub.com/tea

Timp-1, *Col I*, *Col III*, *TGF-β1*, *MMP2*, and *18s* ribosomal housekeeping were used to quantify the expression of desired matrix and matrix regulatory genes (Supplementary Table S1). Samples were incubated at 95°C for 4 min, followed by 40 cycles of denaturation, annealing, and elongation at 95°C, 55°C, and 72°C, respectively. TaqMan fluorescence was measured at the end of the extension step each cycle. Experimental group samples were normalized to *18s* and then referenced to the contralateral normal limb. Gene expression levels are reported as fold change using the $2^{-(\Delta\Delta Ct)}$ method.

Data analysis

Based on an *a priori* power analysis, the implantation of eight animals per group was determined to be sufficient to detect a 15% increase in contractile force between treatment and control animals. This level of detection was designed to detect physiologically relevant and functionally meaningful increases in muscle contractile force. Pilot testing mean and standard deviation contractile force values (2.10 ± 0.15 N/kg) collected from intact TA muscle samples were used. All data are represented by the mean and standard error unless noted. Data were tested for normality using the Shapiro–Wilk Test. Comparisons between treatment groups (VML, DSM, and DSM + MM) for each of the outcome measures (peak force, muscle mass, collagen I% area, and gene expression) were evaluated with a one-way analysis of variance using a commercial statistical software package (JMP). *Post hoc* comparisons were made using Tukey's test. A standard 0.05 level of significance was used for all statistical tests.

Results

Average DSM sample DNA content (1.0 ± 0.1 ng of DNA/mg of tissue) was well below the preferred implantation threshold (<50–70 ng/mg) reported by others.[24,25] Isolated DSM implantation took ~30 min to complete. The addition of MM preparation and coating steps added ~10 min to the procedure. Both DSM and DSM + MM treatment groups tolerated the implantation surgery well. All animals gained weight throughout the observation period at a rate (8.3 ± 0.5 and 8.5 ± 0.3 g/week) that was not significantly different from unrepaired VML defect animals (8.8 ± 0.6 g/week). There were no signs of postsurgical infection. At 1 week postimplantation, all animals were fully ambulatory with no noticeable gait differences between groups. Carprofen dietary gel cups were typically consumed within the first 3 days of surgery (effective dosage [5/mg/kg/day]). All animals reached the 12-week study end point without complications.

After the 12-week recovery period, bilateral measurements of the isometric TA muscle tetanic contractile force were obtained. Tetanic contraction plots for all muscles were characterized by a sharp rise in force, followed by a plateau at the peak force, and then a return to a no force resting state (Fig. 3). The average peak tetanic force produced by normal contralateral TA muscles was 2.0 ± 0.1 N/kg when normalized to animal mass. Following VML injury without repair, the average peak tetanic force dropped to 1.4 ± 0.1 N/kg, which is equivalent to 62 ± 3% of normal contralateral TA muscle values, a statistically significant reduction ($p < 0.05$). Following repair with isolated DSM, TA muscles produced an average contractile force of 1.5 ± 0.1 N/kg, which represents a 17% recovery of the peak force compared to the unrepaired VML muscle group. Although elevated, the peak force recovery following isolated DSM repair was not statistically significant compared to the unrepaired VML group. In response to repair with combined DSM + MM, the average peak tetanic force increased to 1.7 ± 0.2 N/kg, which represents a 50% recovery in force production compared to unrepaired VML values. The recovery of peak tetanic force following DSM + MM repair was statistically significant compared to the unrepaired VML group ($p < 0.05$).

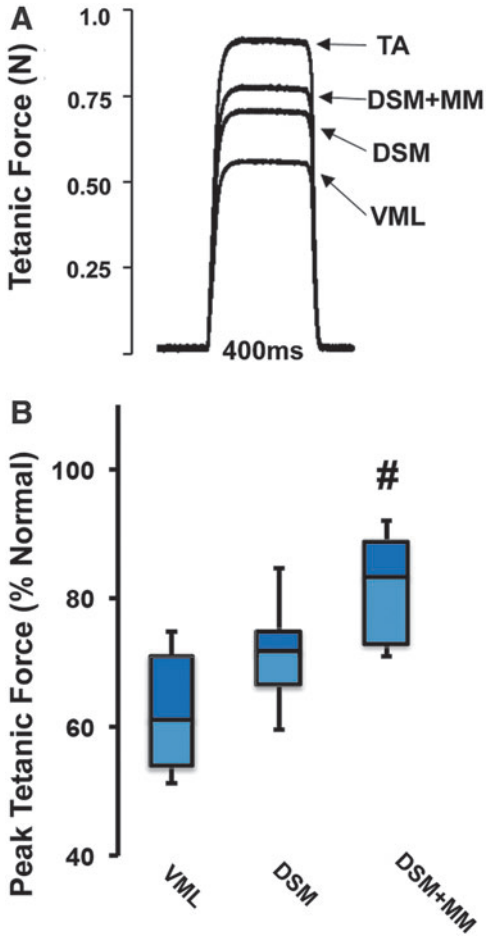

FIG. 3. Twelve weeks after treatment, TA peak contractile force was assessed for both unrepaired and DSM repaired groups ($n = 8$/group). Representative tetanic force responses for normal, unrepaired VML, DSM, and DSM + MM repaired TA muscles **(A)**. Peak tetanic force was normalized to animal weight (N/kg) and computed as a percentage of the untreated contralateral limb for each animal tested **(B)**. Box and whisker plot values shown are the median, first and third quartile, as well as maximum and minimum. The increase in peak contractile force in response to DSM + MM implantation was statically significant compared to both unrepaired VML and isolated DSM repaired samples. ($n = 7$–8/sample group). #Distinguishes significant difference from VML group. $p < 0.05$; ANOVA with *post hoc* Tukey's test. ANOVA, analysis of variance. Color images available online at www.liebertpub.com/tea

For all muscles harvested, there was no evidence of implant site infection or gross deformity at the treatment site following 12 weeks of recovery. Generally, each of the treatment group muscles appeared smaller than contralateral normal muscle and the defect site could often be identified grossly (Fig. 4). The muscles repaired with DSM and DSM + MM appeared to

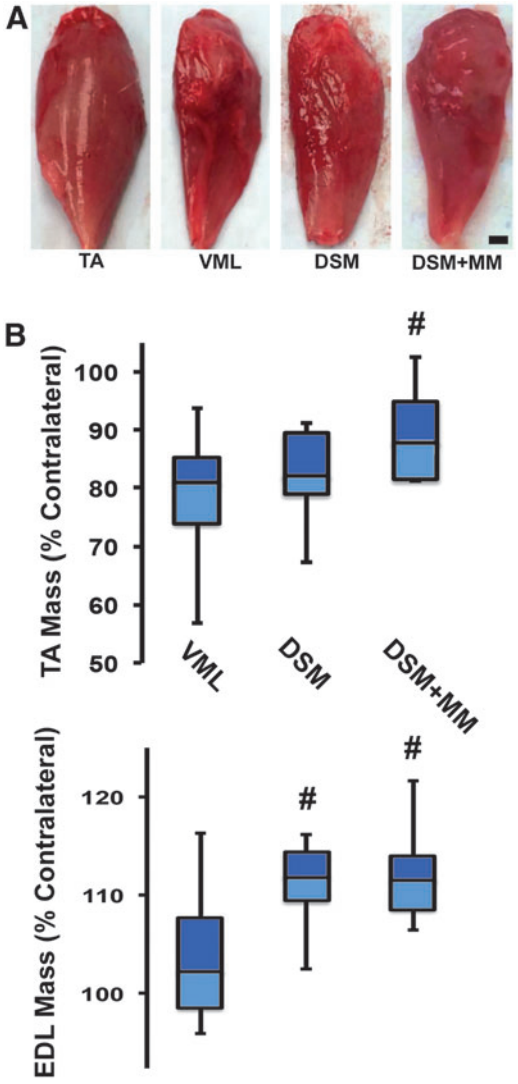

FIG. 4. Gross morphology of normal, unrepaired VML, DSM, and DSM + MM repaired whole TA muscles harvested 12 weeks posttreatment **(A)**. TA weight, calculated as the percent normal contralateral muscle, was significantly increased in response to repair with combined DSM + MM implants **(B)**. The EDL muscle mass was similarly increased in response to treatment, suggesting compensatory hypertrophy. Box and whisker plot values shown are the median, first and third quartile, as well as maximum and minimum. ($n = 8$/sample); #distinguishes significant difference from VML group, $p < 0.05$; ANOVA with *post hoc* Tukey's test. EDL, extensor digitorum longus. Color images available online at www.liebertpub.com/tea

have less fibrosis at the treatment site and less atrophy overall compared to the unrepaired muscles, but still had a less organized surface morphology at the treatment site compared to the ordered striations of normal muscle. Untreated VML sample animals had a body weight normalized average TA mass of 1.27 ± 0.1 g/kg, which is $79 \pm 3\%$ of the contralateral normal TA mass. TA muscle defects repaired with isolated DSM had an average normalized mass of 1.33 ± 0.1 g/kg, which is $82 \pm 3\%$ of contralateral normal muscle mass and represents a 14% recovery in muscle mass compared to the unrepaired VML group. The group of TA muscles repaired with combined DSM + MM had an average mass of 1.40 ± 0.1 g/kg, which is equivalent to $88 \pm 3\%$ of contralateral normal values. DSM + MM muscle mass was significantly increased compared to the unrepaired VML treatment group ($p < 0.05$), but not significantly greater than the isolated DSM repair group. On average, DSM + MM treated muscles recovered 43% of the muscle mass lost following VML injury (79% vs. 88% of normal). Of note, EDL muscles collected from the treated limb were on average larger than contralateral EDL muscles for each treatment group (VML, DSM, and DSM + MM), suggesting compensatory hypertrophy.

At 12 weeks postsurgery, the defect sites were detectable in histological sections prepared from all treatment groups. Transverse histological images of the defect sites for all treatment groups were characterized by the accumulation of repair tissue at the muscle surface (Fig. 5). Unrepaired VML and isolated DSM repair defect site tissues were strongly immunoreactive to αColI, suggesting collagen-enriched connective tissue deposition (fibrosis) at the defect/repair site. Additional ECM proteins, including fibronectin, αColIII, and laminin, were each detected within the repair tissue (Fig. 6). While the general composition of the repair tissue layer was similar across all treatment groups, the size/thickness of the layer was notably different between groups. Specifically, it was generally noted that the repair tissue layer observed in DSM + MM treated sample layer was distinctly thinner than both unrepaired VML and isolated DSM repair groups. The repair layer was often difficult to locate in many tissue sections. For all treatment groups, MHC-positive muscle fibers were present up to the border of the repair layer, but were not observed within the layer itself. For all groups, the collagen dense repair layer was notably thinner (50–500 μm) than the original VML defect (3 mm), suggesting atrophy of the transected muscle tissue proximal and distal to the defect site.

The Masson's Trichrome staining revealed signs of increased collagen deposition (blue staining) around muscle fibers in tissue regions that extended beyond the defect site for both unrepaired VML and isolated DSM repaired tissue sections. Similar qualitative increases in collagen staining were not observed in DSM + MM Masson's stained tissue sections. Subsequent quantitative analysis of αColI immunoreactivity supported the Masson's Trichrome observations. When measured using tissue sections prepared from normal contralateral skeletal muscle samples, collagen I positive immunostaining regions occupied, on average, $6.2 \pm 1.3\%$ of the total tissue section area (Fig. 7). For sections prepared from unrepaired VML and isolated DSM repaired samples, the percent surface area increased to $6.5 \pm 0.8\%$ and $8.6 \pm 0.5\%$ of the total surface area, respectively. The elevated αColI area values detected following isolated DSM repair represent a 33% increase over normal tissue values. Alternatively, DSM + MM repair group collagen I percent area ($5.4 \pm 0.7\%$) was below all other groups, including normal muscle. On average, DSM + MM treated collagen I percent area values were 12% and 37% below VML and isolated DSM repair values, respectively. The difference between DSM + MM and isolated DSM values was statistically significant.

Six key genes associated with ECM structural proteins (*colI* and *ColIII*), ECM regulatory cytokines (TGF-β1, MMP2, and TIMP-1), and myogenesis (MyoD) were examined with the aid of RT-PCR (Fig. 8). Muscle tissue samples collected from both unrepaired VML defect sites and isolated DSM repair sites produced approximately one tenth the relative expression of MyoD compared to normal contralateral

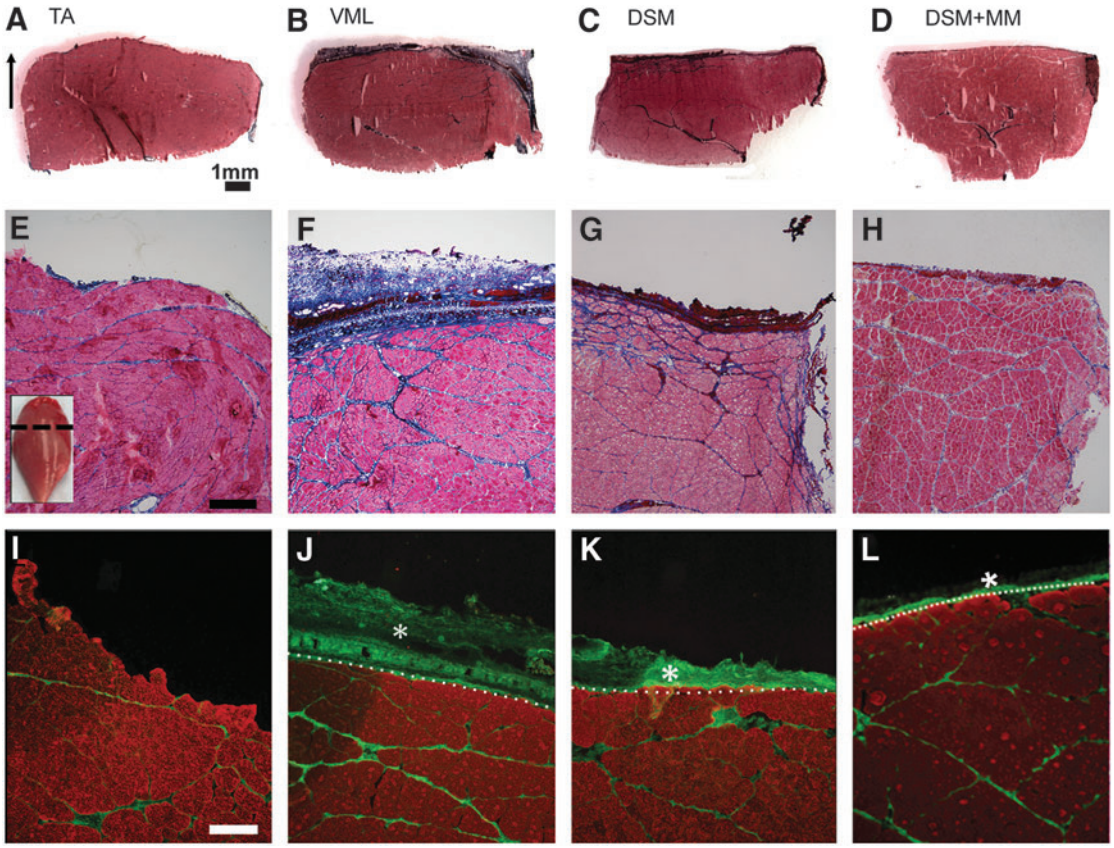

FIG. 5. Representative normal **(A, E, I)**, unrepaired VML **(B, F, J)**, DSM **(C, G, K)**, and DSM + MM **(D, H, L)** repaired histological sections [**(E)** *inset* indicates approximate section location]. Sections were stained with either Masson's Trichrome or immunostained for the presence of MHC (*red*) and collagen type I (*green*). The defect/repair site (*) for unrepaired VML and isolated DSM repaired samples showed evidence of a thick, collagen enriched, connective tissue repair layer. DSM + MM repair site tissue showed markedly less connective tissue formation than VML or DSM groups. *Dotted line* highlights the boundary between collagen dense repair tissue and MHC positive muscle tissue. Scale bar = 250 μm unless noted *Arrow* indicates anterior direction. MHC, myosin heavy chain. Color images available online at www.liebertpub.com/tea

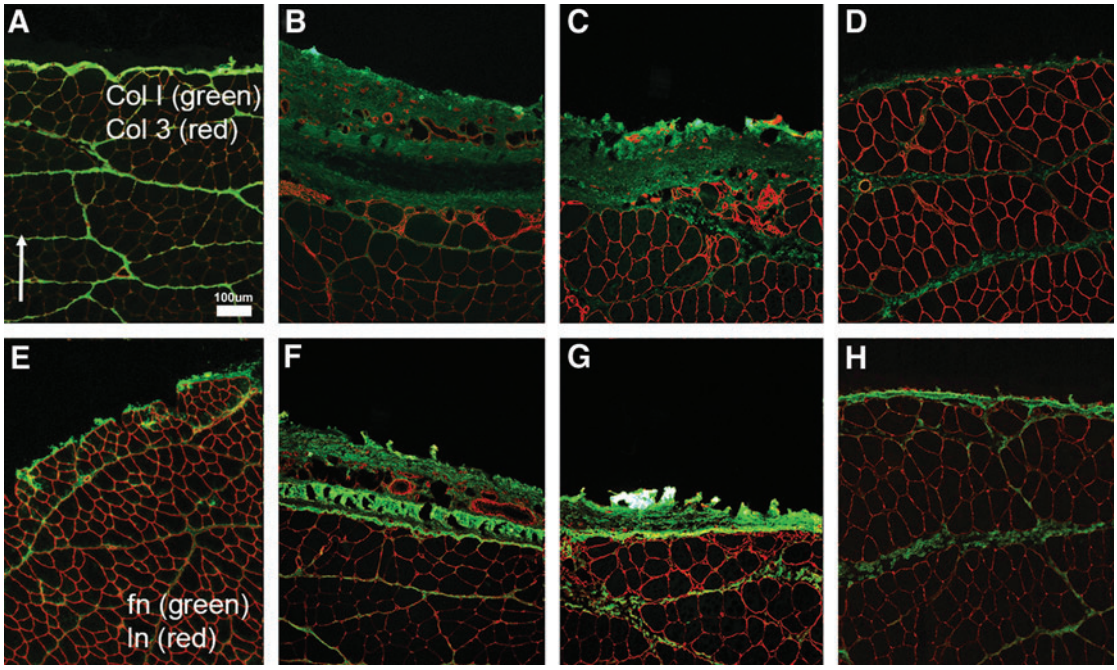

FIG. 6. Representative normal **(A, E)**, unrepaired VML **(B, F)**, DSM **(C, G)**, and DSM + MM **(D, H)** tissue sections. Repair site tissue was immunoreactive to antibodies directed against collagen I and III **(A–D)**, as well as laminin and fibronectin **(E, F)**. Scale bar = 100 μm. *Arrow* indicates anterior direction. Color images available online at www.liebertpub.com/tea

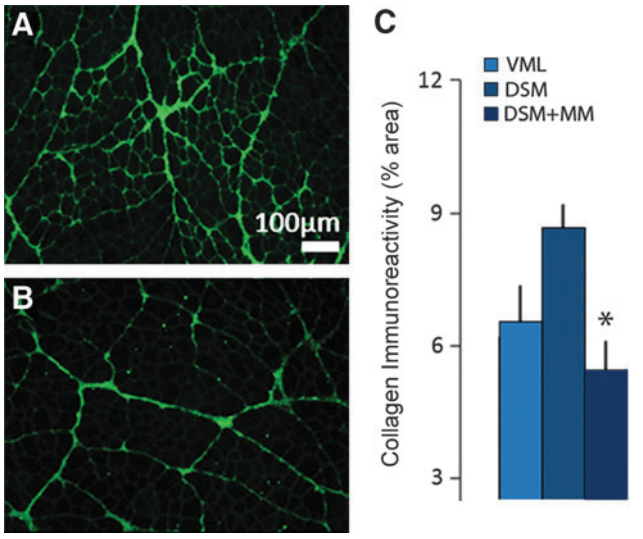

FIG. 7. Representative DSM **(A)** and DSM + MM repaired **(B)** tissue sections immunostained for the presence of collagen type I. The sectional area immunoreactive to collagen type I was calculated using sections prepared from tissue regions located at least 3 mm away from the anterior surface of the muscle. Tissue samples collected from DSM + MM repair samples exhibited a significantly lower immunoreactivity to collagen type I compared to isolated DSM repair samples **(C)**. Scale bar = 100 μm; $n = 3$/sample group; *distinguishes significant difference from the DSM treatment group; $p < 0.05$; ANOVA with Tukey's test. Color images available online at www.liebertpub.com/tea

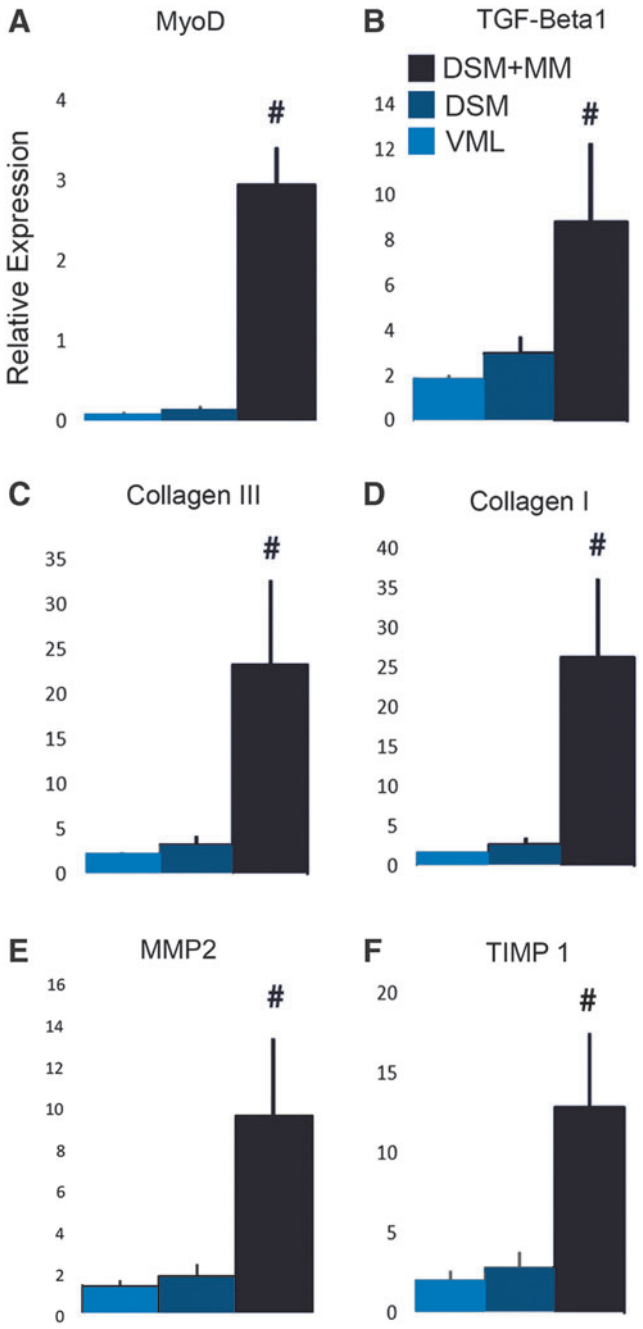

FIG. 8. RT-PCR results (fold change compared to normal muscle) for the ECM structural proteins Collagen I and III, the ECM regulatory cytokines TGF-β1, MMP2, and TIMP-1, and the myogenic marker MyoD. Values shown are mean + SEM; $n = 4$/sample group; #distinguishes significant difference from both VML and DSM groups; $p < 0.05$; ANOVA with Tukey's test. SEM, standard error of the mean. Color images available online at www.liebertpub.com/tea

TA muscle, with fold changes of 0.08 ± 0.04 and 0.14 ± 0.06, respectively. Alternatively, the DSM + MM repaired muscle group produced a statistically significant increase ($p < 0.05$) in the expression of *MyoD* with a fold change of 2.95 ± 0.47 compared to normal TA muscle samples. Analysis of tissue collected from both the VML and isolated DSM repair groups revealed modestly increased structural and regulatory ECM gene expression values compared to normal tissue controls. αColI expression levels measured from unrepaired VML and isolated DSM samples were 1.55 ± 0.14 and 2.60 ± 0.89 of normal muscle, respectively. The expression pattern for each of the ECM regulatory genes followed a similar trend; *MMP2*, *TGF-β*, and *TIMP-1* expression were typically doubled within VML and isolated DSM repair tissue samples. Expression levels for each of the structural and regulatory ECM genes were markedly increased in response to combined DSM + MM repair. The expression level for DSM + MM repaired samples exceeded both the VML and isolated DSM treatment groups by statistically significant margins for each of the genes examined ($p < 0.05$) and was generally an order or magnitude greater than normal contralateral TA tissue expression values.

The gene expression ratios for each of the five ECM genes to the MyoD gene (e.g., *Col I:MyoD*) were calculated across all treatment groups for comparison to normal muscle (Fig. 9). Generally, normal muscle samples produced ECM to MyoD expression ratios that clustered around a value of 13 and ranged from a low of 10 ± 5 (*Col I/MyoD*) to a high of 16 ± 8 (*Col III/MyoD*). Unrepaired VML and isolated DSM repair gene expression ratios were all significantly elevated (3 to 4-fold) in comparison to normal muscle values and clustered between values of 30 and 50. Alternatively, DSM + MM gene expression values were generally lower than normal muscle values ranging from a low of 4 ± 2 (TGF-β1; MyoD) to a high of 11 ± 5 (*Col I/MyoD*). DSM + MM gene expression ratios calculated for *Col I* and *Col III* to *MyoD* were closely matched to normal muscle values and represented the only ratio values across all treatment groups that were not significantly different from normal muscle. The main outcome measures for each of the treatment groups are summarized in Table 1.

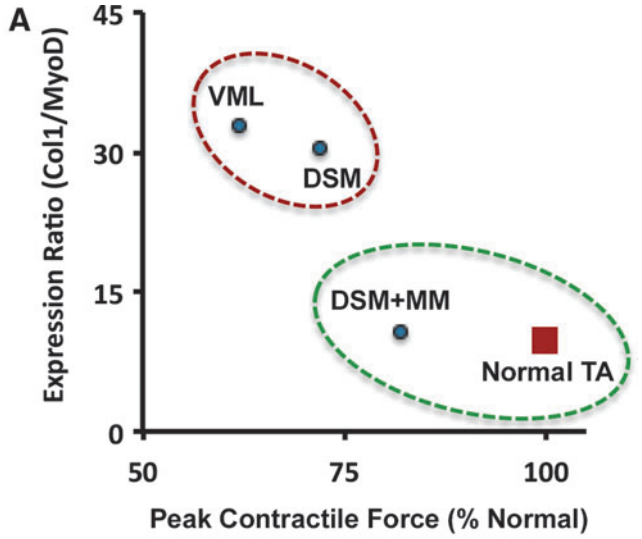

B

	TA	VML	DSM	DSM+MM
TGF-β1 / MyoD	13.7±6.8	41.9±18.0	34.6±12.3	3.6±1.7
Col I / MyoD	9.8±5.3	32.9±10.5	30.3±15.5	10.6±4.5
Col III / MyoD	15.6±7.8	47.1±15.8	38.1±15.3	9.4±4.2
CTGF / MyoD	12.4±5.7	51.5±37.0	28.6±7.3	4.4±2.1
Timp-1 / MyoD	14.6±8.3	45.9±25.2	30.8±12.5	4.9±1.6

FIG. 9. Collagen I to MyoD gene expression ratio versus percent normal contractile force **(A)** for VML, DSM, DSM + MM, and normal TA sample groups. The average expression ratios calculated for VML and DSM samples clustered near an elevated value of 30, while the DSM + MM repair sample ratio was better aligned with normal TA muscle. Average expression ratios **(B)** for each of the ECM structural and ECM regulatory genes to *MyoD*. Expression ratio values shown are mean ± SEM; $n = 4$/sample group. Color images available online at www.liebertpub.com/tea

Discussion

The key findings from this study suggest that the use of an acellular DSM scaffold improved functional recovery from a VML injury and the addition of a MM paste further enhanced regeneration. Specifically, the combination of a DSM scaffold with MM paste restored approximately half the contractile force that was lost to VML injury, a finding that was consistent with the measured increases in TA muscle weight following DSM + MM repair. Secondary findings suggest that the presence of the MM increases myogenesis, indirectly assessed through MyoD expression analysis, and decreased the accumulation of collagen enriched repair tissue at the site of the defect. When taken together the electrophysiological, histological, and gene expression data provided evidence suggesting that the addition of MM to a DSM graft can be utilized to improve muscle regeneration following VML injury.

The infusion bioreactor utilized in this project is a new approach developed by our laboratory to accelerate muscle tissue decellularization. Although perfusion decellularization has been performed on the entire forelimb of a rat[26] and whole organs, such as the liver,[27] heart,[28] kidneys,[29] and lungs,[30] muscle tissue lacks the easily accessible vasculature needed for perfusion, motivating a different approach whereby decellularization solution was infused into the bulk tissue using a needle. In our recently published work, it was demonstrated that DSM scaffolds produced through infusion decellularization retain the composition, mechanics, and architecture of native muscle ECM. The major advantage of our infusion device is that it produces a decellularized scaffold in under 10 h compared to standard diffusion based (incubation with agitation) methods that can take up to two weeks for a similarly sized muscle.[11] Moving forward, a single needle system could be scaled up to create a multineedle infusion device capable of decellularizing bulkier muscle samples needed for large animal models or eventually human tissue for clinical studies. Furthermore, while we currently don't use the infusion process during the DNAse and rinse steps, we could certainly anticipate utilizing the system to accelerate all process steps. Ultimately, we believe the infusion prepared DSM scaffolds are an appropriate material from which to explore VML repair strategies.

The MM codelivery with DSM was initially motivated by findings reported by Corona *et al.*[18] The harvest of MM autografts in a clinical setting makes it an intriguing source of implantable satellite cells for codelivery with DSM. Rather than utilizing satellite cells which are first harvested, purified, expanded, and then ultimately implanted using a two-stage surgical strategy, MM can be acquired and delivered along with allogeneic DSM in a single stage procedure. While a single procedure strategy may simplify surgical

Table 1. Animal Growth; Volumetric Muscle Loss Defect Mass; Decellularized Skeletal Muscle Mass; Peak Contractile Force Normalized to Body Weight and Contralateral Normal Tibialis Anterior; Tibialis Anterior Mass; Extensor Digitorum Longus Mass; and Collagen Type 1 Area Values 12 Weeks After Treatment (Volumetric Muscle Loss, Decellularized Skeletal Muscle, or Decellularized Skeletal Muscle + Minced Muscle)

	Animal growth (g/week)	*Defect mass (mg: wet weight)*	*DSM mass (mg: dry weight)*	*Contractile force (N/kg)*	*Contractile force (% normal TA)*	*TA mass (% normal TA)*	*EDL mass (% normal EDL)*	*Collagen type I (% area)*
VML	8.8 ± 0.6	95 ± 2	NA	1.4 ± 0.1	62 ± 3.5	79 ± 3.1	102 ± 3.0	6.5 ± 0.8
DSM	8.3 ± 0.5	92 ± 2	5.2 ± 0.3	1.5 ± 0.1	71 ± 2.8	82 ± 3.0	110 ± 2.3	8.6 ± 0.5
DSM + MM	8.5 ± 0.3	94 ± 1	4.9 ± 0.3	1.7 ± 0.1[#]	81 ± 3.2[#]	88 ± 3.1[#]	111 ± 2.1[#]	5.4 ± 0.7*

Values are mean ± standard error of the mean. Significant differences (analysis of variance with Tukey's, $p < 0.05$) from VML group distinguished by (#). Significant differences from isolated DSM group distinguished by (*).

VML, volumetric muscle loss; DSM, decellularized skeletal muscle; MM, minced muscle; TA, tibialis anterior; EDL, extensor digitorum longus.

planning, we clearly recognize that the MM volume (25% of the defect mass) utilized in this study, although far less than the full defect size, would still produce harvest challenges and donor site morbidity concerns. To minimize morbidity, it may be possible to collect subcritical muscle biopsies from contralateral muscle sources. Ultimately, the use of a MM grafting may have the greatest utility for the repair of smaller muscles like those of the face[31] and hands[32] where a therapeutic volume of MM muscle could be harvested from the larger muscle of the lower limbs in a manner consistent with the harvest or the middle third of the patellar tendon during anterior cruciate ligament reconstruction.[33]

The encouraging signs of functional regeneration that were observed in response to MM implantation hint at additional cellular implantation factors that may enhance myogenesis within DSM implants. Specifically, the use of MM may do more to enhance muscle regeneration than simply increase the available pool of satellite cells at the injury site. Following muscle sprains and strains, the presence of injured myocytes within the wound site provides pro-regenerative cues. Specifically, it is understood that signaling cascades initiated in response to myofiber injury activate inflammatory and myogenic cells that stimulate the muscle repair process during the essential early phases of regeneration.[34] Inclusion of the signaling cues initiated by myofiber injury may provide opportunities for novel repair strategies. These cues could be provided directly through seeding of DSM scaffolds with myofibers (MM) as was examined in this study, or alternatively by identifying the key chemical signals produced in response to myofiber injury and engineering them into a biomimetic repair strategy.

The selection of a MM graft prepared using 25% of the VML defect mass was motivated by Corona's recent work showing that MM seeded in a collagen hydrogel did not effectively repair VML injury when the mass of MM was prepared using <50% of the tissue collected from the muscle defect.[19] Others have utilized the entire defect to produce significant regenerative results.[18] By exploring the use of a 25% volume MM graft, the low end of what has been explored by others thus far, we hoped to determine whether DSM scaffolds could improve the muscle regenerative performance of MM autografts beyond that which has been achieved to date. The lack of an isolated MM implantation control group was a regrettable shortcoming to this study. It would have been valuable to know the contribution of the MM graft and help elucidate whether the improved functional recovery measured following combined DSM + MM delivery was simply additive or whether there were interaction effects that enhanced regenerative performance when combined. Yet, while the effect of isolated MM was not evaluated in this study, what is clear, is two strategies that showed modest effectiveness when used separately (isolated DSM or <50% MM grafting) and stimulated significant functional muscle recovery when used in combination, suggesting to us that infusion prepared DSM material is a MM carrier scaffold worthy of continued investigation.

Toward this end, an improved understanding of the interactions between the MM paste and DSM scaffold is warranted. In particular, it would be of interest to know whether the DSM scaffolds are serving as simply a carrier material for the delivery of satellite cells or whether the scaffold creates a pro-myogenic environment that enhances satellite cell expansion. DSM + MM interactions could be explored over the short term using *in vitro* models, or *in vivo* utilizing earlier time points. The longer 12-week time point used in this study, while appropriate for the detection of force recovery, missed the key regenerative events that occur during early wound healing. Research suggests that a 1-week time point may be more appropriate for the detection of regenerative satellite cell activity.[35]

The increased effectiveness of the DSM + MM scaffold compared to the collagen hydrogel + MM examined by Corona could potentially be attributed to the architecture of the DSM scaffold. Scaffolds composed of DSM, including the infusion prepared scaffolds explored in this study, are unique because they retain the parallel alignment of the native muscle from which they were obtained.[36] We, as well as others, anticipate that scaffolds with muscle mimetic network alignment will improve muscle regeneration by providing the appropriate topographical cues during healing.[5,37] In whole muscle, ECM surrounds and supports multinucleated myofibers, which are highly aligned in the direction of muscle contraction. The individual fibers range from 5 to 100 μm in diameter and can be as long as several centimeters.[38] During implantation we were careful to orient the DSM scaffolds in the direction of TA contraction. *In vitro* models indicate that muscle progenitor cells utilize alignment cues during myogenesis.[39,40] Similar alignment-sensitive responses have been reported for other cells, including cardiac muscle and tendons.[41,42] Yet, while the many *in vitro* alignment studies support the motivation of aligned regenerative scaffolds, we recognize that *in vivo* evidence indicating that scaffold alignment is critical to muscle implant success does not yet exist. The lack of *in vivo* data supporting the importance of scaffold alignment in muscle regenerative therapies would appear to motivate future studies.

VML repair with DSM + MM dramatically increased gene expression for each of the structural and regulatory ECM genes explored in this study. However, the histological appearance of defect/repair site tissue for both VML and isolated DSM repair groups would suggest that ECM deposition and gene expression should be increased in these groups compared to the DSM + MM group. We suspect that ECM gene expression levels for both VML and isolated DSM groups were elevated during earlier time points; an expression pattern that is consistent with muscle fibrosis.[43] Once a stable fibrotic scar was formed, the genes returned to the lower expression values we measured at 12 weeks. It is also important to note that the collagen I immunoreactivity and PCR analysis were conducted on samples taken from different tissue regions. Collagen immunoreactivity was assessed within tissue regions located distant to the repair/defect site, while the tissue used for PCR analysis was collected from the repair site. As a result, the collagen immunoreactivity measures are likely an indicator of tissue wide ECM adaptation to differences in force generation and transmission between treatment groups,[44] while the PCR results are indicative of the regenerative and remodeling processes occurring at the site of repair.

The PCR data suggest that the addition of MM to DSM scaffolds prolongs myogenesis and ECM production at the repair site following VML injury repair. The increased expression of ECM related genes and MyoD at 12 weeks could be indicative of active remodeling and adaptation at the defect site in response to muscle activity.[45] Alternatively, the prolonged upregulation of ECM genes at 12 weeks could be indicative of

ongoing fibrosis.[46] To determine whether the expression patterns we observed at 12-weeks are beneficial or pathological, longer recovery time points may need to be explored to determine whether contractile recovery is maintained. In addition, it may be of interest to explore gene expression profiles both within and away from the repair site to gain a better understanding of muscle wide responses to each repair scheme.

We explored the ratio of the relative gene expression for each of the ECM genes to MyoD to elucidate differences that may exist between normal muscle homeostasis and each of the treatment groups. The relationships between key repair genes may provide additional insights into the repair process, and in fact gene expression ratios have been utilized to examine tissue healing trends in musculoskeletal tissues, including bone[47] and ligament.[48] In this study, normal TA muscle tissue ratios (ECM:MyoD) ranged between 10 and 15 for each of the ECM genes measured. Repair strategies that increase expression ratios away from normal TA values might suggest a shift in the repair process toward increased ECM production and/or decreased myogenesis. In contrast, repair strategies that cause expression ratios to fall below normal TA values might alternatively suggest a shift toward decreased ECM production and/or increased myogenesis. With that hypothesis in mind, the DSM + MM repaired muscle groups expressed ratios that were at or below normal muscle for each of the genes tested. Conversely, muscles that received VML defects and those that were repaired with isolated DSM had ratios ranging from 32.9–51.5 to 28.6–38.1, respectively. Potentially, these and other gene expression ratios could be used to evaluate VML repair strategies in future animal models and may provide insights into treatment strategies that target gene pairs.

The codelivery of DSM with MM restored approximately half of the peak contractile force lost following VML injury (81% vs. 62%). The question then remains; what additional strategies could be utilized to restore the last 20%? Existing animal studies show that physical rehabilitation in the form of voluntary wheel running after VML injury and subsequent MM transplant can improve maximal isometric torque, without causing significant damage to healing muscle.[18] These results suggest that the application of force to the repair site during healing can contribute to muscle regeneration. This is supported by *in vitro* findings that have shown that force and substrate strain enhance muscle progenitor cell myogenesis.[49,50] Motivated by a desire to closely replicate previously reported MM treatment strategies, DSM implants were not sutured to the surrounding TA muscle tissue during implantation. In the future, we plan to incorporate surgical attachment into the repair strategy, as it will enable the transfer of contractile force through the repair site during healing and regeneration. In addition to physical stimuli, the delivery of soluble stimuli in the form of growth factors has been found to enhance functional recovery after muscle injury. Specifically, fibroblast growth factor, insulin growth factor, and nerve growth factor have been shown to aid in muscle regeneration.[51] If necessary, these key molecules could be injected into the repair site at the time of surgery to deliver short-term effects, or physically linked to DSM scaffolds to potentially prolong their myogenic activity.[52]

The Fischer 344 rats used in this study had not reached skeletal maturity and continued to gain weight throughout the recovery period. As a result, the findings reported in this study might more accurately model the response of young adults to VML repair with DSM and MM implants. Surgical muscle removal resulting from soft tissue sarcoma resection is another anticipated target for VML repair strategies like that described in this study.[53] This group of patients is typically older, and to date the regenerative response of MM in an aged model has not been investigated. Age related changes in muscle biology might be a limiting factor for MM usage in older patients. It is well established that muscle resident satellite cells account for the majority of skeletal muscle's regenerative capacity.[54] However, aging leads to an overall decrease in myogenic capacity mostly, in part, due to reduced satellite cell activity.[54–56] In future studies, it would be useful to understand whether the regenerative benefits of MM autografts are maintained when harvested from aged muscle. Yet, while the use of MM autografts may not be suitable for all VML repair scenarios, the findings reported herein add to the growing body of evidence supporting its potential as a VML treatment strategy that warrants continued investigation.

Conclusions

The key findings of this study suggest that:

1. The addition of MM to DSM significantly increased peak TA tetanic contractile force compared to unrepaired VML controls.
2. DSM + MM repair significantly increased TA muscle mass, restoring approximately half of the muscle mass lost to VML injury.
3. Histological analysis revealed a reduced fibrotic response at the repair site in response to DSM + MM repairs, compared to either unrepaired VML or isolated DSM repair strategies.
4. *MyoD*, ECM (*Col I* and *Col III*), and ECM regulatory (*TGF-β1*, CTGF, and *TIMP-1*) gene expression levels were significantly increased over all other treatment groups in response to DSM + MM repair.
5. Analysis of gene expression ratios may provide a useful indicator of VML treatment efficacy and restoration of normal muscle homeostasis.

Acknowledgments

Research reported in this publication was supported by the National Institute of Arthritis and Musculoskeletal and Skin Diseases of the National Institutes of Health under Award Number R15AR064481 and the Arkansas Biosciences Institute.

Disclosure Statement

No competing financial interests exist.

References

1. Terada, N., Takayama, S., Yamada, H., and Seki, T. Muscle repair after a transsection injury with development of a gap: an experimental study in rats. Scand J Plast Reconstr Surg Hand Surg **35,** 233, 2001.
2. Oishi, S.N., and Ezaki, M. Free gracilis transfer to restore finger flexion in Volkmann ischemic contracture. Tech Hand Up Extrem Surg **14,** 104, 2010.

3. Terzis, J.K., and Kostopoulos, V.K. Free muscle transfer in posttraumatic plexopathies: part 1: the shoulder. Ann Plast Surg **65,** 312, 2010.
4. Vekris, M.D., Beris, A.E., Lykissas, M.G., Korompilias, A.V., Vekris, A.D., and Soucacos, P.N. Restoration of elbow function in severe brachial plexus paralysis via muscle transfers. Injury **39 Suppl 3,** S15, 2008.
5. Bian, W., and Bursac, N. Engineered skeletal muscle tissue networks with controllable architecture. Biomaterials **30,** 1401, 2009.
6. Chiron, S., Tomczak, C., Duperray, A., Laine, J., Bonne, G., Eder, A., Hansen, A., Eschenhagen, T., Verdier, C., and Coirault, C. Complex interactions between human myoblasts and the surrounding 3D fibrin-based matrix. PloS One **7,** e36173, 2012.
7. Hurd, S.A., Bhatti, N.M., Walker, A.M., Kasukonis, B.M., and Wolchok, J.C. Development of a biological scaffold engineered using the extracellular matrix secreted by skeletal muscle cells. Biomaterials **49,** 9, 2015.
8. Juhas, M., Engelmayr, G.C., Jr., Fontanella, A.N., Palmer, G.M., and Bursac, N. Biomimetic engineered muscle with capacity for vascular integration and functional maturation in vivo. Proc Natl Acad Sci U S A **111,** 5508, 2014.
9. Wilson, K., Terlouw, A., Roberts, K., and Wolchok, J.C. The characterization of decellularized human skeletal muscle as a blueprint for mimetic scaffolds. J Mater Sci Mater Med **27,** 125, 2016.
10. Corona, B.T., Ward, C.L., Baker, H.B., Walters, T.J., and Christ, G.J. Implantation of in vitro tissue engineered muscle repair constructs and bladder acellular matrices partially restore in vivo skeletal muscle function in a rat model of volumetric muscle loss injury. Tissue Eng Part A **20,** 705, 2014.
11. Merritt, E.K., Cannon, M.V., Hammers, D.W., Le, L.N., Gokhale, R., Sarathy, A., Song, T.J., Tierney, M.T., Suggs, L.J., Walters, T.J., and Farrar, R.P. Repair of traumatic skeletal muscle injury with bone-marrow-derived mesenchymal stem cells seeded on extracellular matrix. Tissue Eng Part A **16,** 2871, 2010.
12. Perniconi, B., Costa, A., Aulino, P., Teodori, L., Adamo, S., and Coletti, D. The pro-myogenic environment provided by whole organ scale acellular scaffolds from skeletal muscle. Biomaterials **32,** 7870, 2011.
13. Wolf, M.T., Daly, K.A., Reing, J.E., and Badylak, S.F. Biologic scaffold composed of skeletal muscle extracellular matrix. Biomaterials **33,** 2916, 2012.
14. Mase, V.J., Jr., Hsu, J.R., Wolf, S.E., Wenke, J.C., Baer, D.G., Owens, J., Badylak, S.F., and Walters, T.J. Clinical application of an acellular biologic scaffold for surgical repair of a large, traumatic quadriceps femoris muscle defect. Orthopedics **33,** 511, 2010.
15. Sicari, B.M., Rubin, J.P., Dearth, C.L., Wolf, M.T., Ambrosio, F., Boninger, M., Turner, N.J., Weber, D.J., Simpson, T.W., Wyse, A., Brown, E.H., Dziki, J.L., Fisher, L.E., Brown, S., and Badylak, S.F. An acellular biologic scaffold promotes skeletal muscle formation in mice and humans with volumetric muscle loss. Sci Transl Med **6,** 234ra58, 2014.
16. Kasukonis, B., Kim, J., Washington, T., and Wolchok, J. Development of an infusion bioreactor for the accelerated preparation of decellularized skeletal muscle scaffolds. Biotechnol Prog **32,** 745, 2016.
17. Aurora, A., Roe, J.L., Corona, B.T., and Walters, T.J. An acellular biologic scaffold does not regenerate appreciable de novo muscle tissue in rat models of volumetric muscle loss injury. Biomaterials **67,** 393, 2015.
18. Corona, B.T., Garg, K., Ward, C.L., McDaniel, J.S., Walters, T.J., and Rathbone, C.R. Autologous minced muscle grafts: a tissue engineering therapy for the volumetric loss of skeletal muscle. Am J Physiol Cell Physiol **305,** C761, 2013.
19. Ward, C.L., Ji, L., and Corona, B.T. An autologous muscle tissue expansion approach for the treatment of volumetric muscle loss. BioRes Open Access **4,** 198, 2015.
20. Wu, X., Corona, B.T., Chen, X., and Walters, T.J. A standardized rat model of volumetric muscle loss injury for the development of tissue engineering therapies. Biores Open Access **1,** 280, 2012.
21. Kim, J.T., Kasukonis, B.M., Brown, L.A., Washington, T.A., and Wolchok, J.C. Recovery from volumetric muscle loss injury: a comparison between young and aged rats. Exp Gerontol **83,** 37, 2016.
22. Bedair, H., Liu, T.T., Kaar, J.L., Badlani, S., Russell, A.J., Li, Y., and Huard, J. Matrix metalloproteinase-1 therapy improves muscle healing. J Appl Physiol **102,** 2338, 2007.
23. Washington, T.A., Brown, L., Smith, D.A., Davis, G., Baum, J., and Bottje, W. Monocarboxylate transporter expression at the onset of skeletal muscle regeneration. Physiol Rep **1,** e00075, 2013.
24. Crapo, P.M., Gilbert, T.W., and Badylak, S.F. An overview of tissue and whole organ decellularization processes. Biomaterials **32,** 3233, 2011.
25. Zhang, Y., He, Y., Bharadwaj, S., Hammam, N., Carnagey, K., Myers, R., Atala, A., and Van Dyke, M. Tissue-specific extracellular matrix coatings for the promotion of cell proliferation and maintenance of cell phenotype. Biomaterials **30,** 4021, 2009.
26. Jank, B.J., Xiong, L., Moser, P.T., Guyette, J.P., Ren, X., Cetrulo, C.L., Leonard, D.A., Fernandez, L., Fagan, S.P., and Ott, H.C. Engineered composite tissue as a bioartificial limb graft. Biomaterials **61,** 246, 2015.
27. Uygun, B.E., Soto-Gutierrez, A., Yagi, H., Izamis, M.L., Guzzardi, M.A., Shulman, C., Milwid, J., Kobayashi, N., Tilles, A., Berthiaume, F., Hertl, M., Nahmias, Y., Yarmush, M.L., and Uygun, K. Organ reengineering through development of a transplantable recellularized liver graft using decellularized liver matrix. Nat Med **16,** 814, 2010.
28. Ott, H.C., Matthiesen, T.S., Goh, S.K., Black, L.D., Kren, S.M., Netoff, T.I., and Taylor, D.A. Perfusion-decellularized matrix: using nature's platform to engineer a bioartificial heart. Nat Med **14,** 213, 2008.
29. Sullivan, D.C., Mirmalek-Sani, S.H., Deegan, D.B., Baptista, P.M., Aboushwareb, T., Atala, A., and Yoo, J.J. Decellularization methods of porcine kidneys for whole organ engineering using a high-throughput system. Biomaterials **33,** 7756, 2012.
30. Ott, H.C., Clippinger, B., Conrad, C., Schuetz, C., Pomerantseva, I., Ikonomou, L., Kotton, D., and Vacanti, J.P. Regeneration and orthotopic transplantation of a bioartificial lung. Nat Med **16,** 927, 2010.
31. Cardenas-Mejia, A., Covarrubias-Ramirez, J.V., Bello-Margolis, A., and Rozen, S. Double innervated free functional muscle transfer for facial reanimation. J Plast Surg Hand Surg **49,** 183, 2015.
32. Lin, C.H., Zhu, Z.S., Lin, C.H., Hsu, C.C., Yeh, J.T., and Lin, Y.T. Primary free functioning muscle transfer for fingers with accompanying tendon transfer for thumb provide one-stage upper extremity composite reconstruction in acute open wound. J Trauma Acute Care Surg **72,** 737, 2012.
33. McGuire, D.A., and Wolchok, J.C. Consistent and accurate graft passage and interference screw guide wire placement

during single incision anterior cruciate ligament reconstruction. Arthroscopy **13,** 526, 1997.
34. McClung, J.M., Davis, J.M., and Carson, J.A. Ovarian hormone status and skeletal muscle inflammation during recovery from disuse in rats. Exp Physiol **92,** 219, 2007.
35. Tian, Z.L., Jiang, S.K., Zhang, M., Wang, M., Li, J.Y., Zhao, R., Wang, L.L., Li, S.S., Liu, M., Zhang, M.Z., and Guan, D.W. Detection of satellite cells during skeletal muscle wound healing in rats: time-dependent expressions of Pax7 and MyoD in relation to wound age. Int J Legal Med **130,** 163, 2016.
36. Hinds, S., Bian, W., Dennis, R.G., and Bursac, N. The role of extracellular matrix composition in structure and function of bioengineered skeletal muscle. Biomaterials **32,** 3575, 2011.
37. Lam, M.T., Huang, Y.C., Birla, R.K., and Takayama, S. Microfeature guided skeletal muscle tissue engineering for highly organized 3-dimensional free-standing constructs. Biomaterials **30,** 1150, 2009.
38. Maier, F., and Bornemann, A. Comparison of the muscle fiber diameter and satellite cell frequency in human muscle biopsies. Muscle Nerve **22,** 578, 1999.
39. Jana, S., Leung, M., Chang, J., and Zhang, M. Effect of nano- and micro-scale topological features on alignment of muscle cells and commitment of myogenic differentiation. Biofabrication **6,** 035012, 2014.
40. Patel, A., Mukundan, S., Wang, W., Karumuri, A., Sant, V., Mukhopadhyay, S.M., and Sant, S. Carbon-based hierarchical scaffolds for myoblast differentiation: synergy between nano-functionalization and alignment. Acta Biomater **32,** 77, 2016.
41. English, A., Azeem, A., Spanoudes, K., Jones, E., Tripathi, B., Basu, N., McNamara, K., Tofail, S.A., Rooney, N., Riley, G., O'Riordan, A., Cross, G., Hutmacher, D., Biggs, M., Pandit, A., and Zeugolis, D.I. Substrate topography: a valuable in vitro tool, but a clinical red herring for in vivo tenogenesis. Acta Biomater **27,** 3, 2015.
42. Morez, C., Noseda, M., Paiva, M.A., Belian, E., Schneider, M.D., and Stevens, M.M. Enhanced efficiency of genetic programming toward cardiomyocyte creation through topographical cues. Biomaterials **70,** 94, 2015.
43. Davis, M.E., Korn, M.A., Gumucio, J.P., Harning, J.A., Saripalli, A.L., Bedi, A., and Mendias, C.L. Simvastatin reduces fibrosis and protects against muscle weakness after massive rotator cuff tear. J Shoulder Elbow Surg **24,** 280, 2015.
44. Hjorth, M., Norheim, F., Meen, A.J., Pourteymour, S., Lee, S., Holen, T., Jensen, J., Birkeland, K.I., Martinov, V.N., Langleite, T.M., Eckardt, K., Drevon, C.A., and Kolset, S.O. The effect of acute and long-term physical activity on extracellular matrix and serglycin in human skeletal muscle. Physiol Rep **3,** pii: e12473, 2015.
45. Hyldahl, R.D., Nelson, B., Xin, L., Welling, T., Groscost, L., Hubal, M.J., Chipkin, S., Clarkson, P.M., and Parcell, A.C. Extracellular matrix remodeling and its contribution to protective adaptation following lengthening contractions in human muscle. FASEB J **29,** 2894, 2015.
46. Mann, C.J., Perdiguero, E., Kharraz, Y., Aguilar, S., Pessina, P., Serrano, A.L., and Munoz-Canoves, P. Aberrant repair and fibrosis development in skeletal muscle. Skelet Muscle **1,** 21, 2011.
47. Chow, S.K., Leung, K.S., Qin, L., Wei, F., and Cheung, W.H. Callus formation is related to the expression ratios of estrogen receptors-alpha and -beta in ovariectomy-induced osteoporotic fracture healing. Arch Orthopaed Trauma Surg **134,** 1405, 2014.
48. Canseco, J.A., Kojima, K., Penvose, A.R., Ross, J.D., Obokata, H., Gomoll, A.H., and Vacanti, C.A. Effect on ligament marker expression by direct-contact co-culture of mesenchymal stem cells and anterior cruciate ligament cells. Tissue Eng Part A **18,** 2549, 2012.
49. Egusa, H., Kobayashi, M., Matsumoto, T., Sasaki, J., Uraguchi, S., and Yatani, H. Application of cyclic strain for accelerated skeletal myogenic differentiation of mouse bone marrow-derived mesenchymal stromal cells with cell alignment. Tissue Eng Part A **19,** 770, 2013.
50. Heher, P., Maleiner, B., Pruller, J., Teuschl, A.H., Kollmitzer, J., Monforte, X., Wolbank, S., Redl, H., Runzler, D., and Fuchs, C. A novel bioreactor for the generation of highly aligned 3D skeletal muscle-like constructs through orientation of fibrin via application of static strain. Acta Biomater **24,** 251, 2015.
51. Baoge, L., Van Den Steen, E., Rimbaut, S., Philips, N., Witvrouw, E., Almqvist, K.F., Vanderstraeten, G., and Vanden Bossche, L.C. Treatment of skeletal muscle injury: a review. ISRN Orthoped **2012,** 689012, 2012.
52. Ramazanoglu, M., Lutz, R., Rusche, P., Trabzon, L., Kose, G.T., Prechtl, C., and Schlegel, K.A. Bone response to biomimetic implants delivering BMP-2 and VEGF: an immunohistochemical study. J Craniomaxillofac Surg **41,** 826, 2013.
53. Fischer, S., Soimaru, S., Hirsch, T., Kueckelhaus, M., Seitz, C., Lehnhardt, M., Goertz, O., Steinau, H.U., and Daigeler, A. Local tendon transfer for knee extensor mechanism reconstruction after soft tissue sarcoma resection. J Plast Reconstr Aesthet Surg **68,** 729, 2015.
54. Conboy, I.M., and Rando, T.A. Aging, stem cells and tissue regeneration: lessons from muscle. Cell Cycle **4,** 407, 2005.
55. Brack, A.S., and Rando, T.A. Intrinsic changes and extrinsic influences of myogenic stem cell function during aging. Stem Cell Rev **3,** 226, 2007.
56. Snow, M.H. The effects of aging on satellite cells in skeletal muscles of mice and rats. Cell Tissue Res **185,** 399, 1977.

Address correspondence to:
Jeffrey Wolchok, PhD
Department of Biomedical Engineering
College of Engineering
University of Arkansas
125 Engineering Hall
Fayetteville, AR 72701

E-mail: jwolchok@uark.edu

Received: April 6, 2016
Accepted: August 24, 2016
Online Publication Date: September 23, 2016